Multimedia Tools and Applications (2023) 82:44859–44883
https://doi.org/10.1007/s11042-023-16651-9

Multi-focus image fusion by using swarm and physics based metaheuristic algorithms: a comparative study with archimedes, atomic orbital search, equilibrium, particle swarm, artificial bee colony and jellyfish search optimizers

Fatma Çakıroğlu[1] · Rifat Kurban[2] · Ali Durmuş[3] · Ercan Karaköse[4]

Received: 27 December 2022 / Revised: 11 August 2023 / Accepted: 23 August 2023 /
Published online: 7 September 2023

Abstract
The lenses focus only on the objects at a specific distance when an image is captured, the objects at other distances look blurred. This is referred to as the limited depth of field problem, and several attempts exist to solve this problem. Multi-focus image fusion is one of the most used methods when solving this problem. A clear image of the whole scene is obtained by fusing at least two different images obtained with different focuses. Block-based methods are one of the most used methods for multi-focus fusion at the pixel-level. The size of the block to be used is an important factor for determining the performance of the fusion. Thus, the block size must be optimized. In this study, the comparison between the swarm-based and physics-based algorithms is made to determine the optimal block size. The comparison has been made among the following optimization methods which are, namely, Archimedes Optimization Algorithm (AOA), Atomic Orbital Search (AOS) and Equilibrium Optimizer (EO) from the physics-based algorithms and Particle Swarm Optimization (PSO), Artificial Bee Colony (ABC) and Jellyfish Search Algorithm (JSA) from swarm-based algorithms. The swarm-based ABC and JSA algorithms have shown a better performance when compared to physics-based methods. Moreover, meta-heuristic algorithms, in general, are more adaptive compared to the traditional fusion methods.

Keywords Multi-focus image fusion · Swarm-based optimization algorithm · Physics-based optimization algorithms

✉ Rifat Kurban
rifat.kurban@agu.edu.tr

[1] Department of Electrical and Electronics Engineering, Institute of Graduate Education, Kayseri University, Kayseri, Türkiye

[2] Department of Computer Engineering, Engineering Faculty, Abdullah Gul University, Kayseri, Türkiye

[3] Department of Electrical and Electronics Engineering, Engineering & Architecture and Design Faculty, Kayseri University, Kayseri, Türkiye

[4] Department of Natural Sciences, Engineering & Architecture and Design Faculty, Kayseri University, Kayseri, Türkiye

1 Introduction

While obtaining the image of an object at a specific distance, optical lenses focus only on some part of the scene and therefore the objects that are at other distances cannot be focused by the lens. This is called the limited depth of field problem of optical lenses [1]. Due to the limited depth of field problem, the optical lenses cannot focus on the whole scene. While capturing the images of the objects that are in focus, the other objects, which are out of focus, look blurred in the image [2]. This problem can be solved by fusing at least two different images of a scene obtained by different focuses, using image processing methods. The fused image, obtained by fusing multiple input images using different fusion methods, contains more information compared to the input images [3, 4]. Multi-focus image fusion has many different fields of applications. It is used in several fields such as microscopic and medical imaging, computer vision, remote sensing, visual sensor arrays, and optical microscopy [5–11]. Several fusion methods are examined deeply in review studies [12, 13]. Multi-focus image fusion methods are classified into four groups, namely; transformation domain methods, spatial domain methods, deep learning-based methods, and hybrid methods where the advantages of transformation domain and spatial domain methods are combined [13]. In the transformation domain based methods, the input image is transformed into another domain in order to be fused more effectively [14]. In order to utilize the information at multiple resolutions and different scales, the input images are transformed by using the pyramid transformation or wavelet transform and then the fused image is created [12]. However, the implementation of these methods is complicated and the algorithms are time-consuming and these approaches are generally shift-variant [12, 13].

In the pixel-based image fusion methods, the completely clear fused image is obtained by selecting the sharp pixels after performing the sharpness analysis for each pixel [15]. The focus criterion functions are very important in pixel based fusion methods [16]. One of the benefits of these methods is that they allow for the preservation of all pixels in the fused region, ensuring that no information is lost [17]. Moreover, spatial domain techniques are unaffected by shifts in position and can handle issues with moving objects and misaligned source images. They are also efficient to implement because they do not involve any type of transformation, instead performing all operations at the pixel level in the spatial domain [12, 13].

Li et al. proposed a method based on pixel visibility [18]. Another method that is based on combining the focus maps obtained by block-based focus measures and employing a multi matting model with weight maps is proposed by Chen et al. [19]. Xia et al. proposed a method to classify the misdescribed pixels into two categories namely the concentrated and diffused sets [20]. Different block-based image fusion methods are proposed to enhance the quality of the fused image and these methods aim to select blocks that are clearer from the input images and create a sharper image. Aslantas and Kurban presented an image fusion method based on Frequency Selective Weighted Median (FSWM) filter [21]. The method of Pulse Coupled Neural Network (PCNN) which is based on block division is proposed by Huang and Jing [22] A multifocal image fusion method based on placing blocks in optimal positions by taking into account the clear regions of the source images is presented in the literature by Toprak and Aslantaş [23]. Aslantaş and Toprak obtained composite images by calculating the point distribution functions of source images with a technique based on differential evolution algorithm [24]. Discrete Wavelet Transform (DWT), one of the well-known traditional transform-based methods in the literature, was developed by setting

different fusion rules to combine low frequency and high frequency coefficients [25, 26]. The Stationary Wavelet Transform (SWT) method is similar to the DWT in that single subsampling is suppressed processing [27, 28]. Discrete Cosine Transform (DCT), one of the transform-based methods, divides the images into $N \times N$ size blocks and calculates the discrete cosine transform coefficients for each block. Blocks suitable for the fusion rule are selected and combined coefficient values are generated. Inverse discrete cosine transform is applied to the combined coefficient values [29]. Discrete cosine harmonic wavelet transform (DCHWT) based multifocal image fusion method is proposed by Kumar to preserve the visual quality and performance of the fused image with reduced computations [30]. Vakaimalar et al. proposed a method for image fusion based on the integration of spatial frequency and DCT [31]. Various multifocal image fusion methods based on DCT have been proposed [32–34]. Another method used in image fusion is Principal Component Analysis (PCA). PCA is a statistical technique. It is vector based [29, 35]. In block-based image fusion methods, it is undesirable to have block sizes that are too small or too big. The blocks that have a fixed size may not be suitable for every application. Therefore, the optimization of the block size is required. Artificial intelligence optimization algorithms have good performance to solve the image fusion problem. Bouzos et al. have worked on a method centered on conditional random field optimization [36]. Genetic algorithm for multi-focus based image fusion is proposed by Kong et al. [37]. Aslantas and Kurban have suggested a multi-focus algorithm focused on differential evolution algorithm to optimize the block size [38]. Banharnsakun et al. proposed a multi-focus image fusion method with Artificial Bee Colony (ABC) algorithm [39]. ABC based method has shown better performance compared to other existing methods. It has been presented by Çıtıl et al. that the Jellyfish search algorithm (JSA) based on block-based image fusion method has better results compared to traditional fusion methods [40]. Quality metrics in the literature are used to compare multi-focus image fusion algorithms. One such metric is called a weighted focus measure. An advanced algorithm based on this metric has been proposed by Derui Ding et al. [41].

In this study, the most widely known physics-based and swarm-based optimization algorithms to solve the multi-focus image fusion problem are compared. In the experiments, the Archimedes Optimization Algorithm (AOA) [42], Atomic Orbital Search (AOS) [43] and Equilibrium Optimizer (EO) [44] are used as physics-based algorithms to solve the multi-focus image fusion problem. In addition to that, the Particle Swarm Optimization (PSO) [45], Artificial Bee Colony (ABC) [46] and Jellyfish Search Algorithm (JSA) [47] are used as swarm-based algorithms. The rest of the paper has been organized as follows: Section 2 briefly introduces the block-based multi-focus image fusion method by using metaheuristic algorithms. Sections 3 and 4 give information about the physics-based and the swarm-based algorithms, respectively. Quality metrics are given in Section 5 and Section 6 contains the experiments and the evaluation of the results. In Section 7, the paper is concluded.

2 Multi-focus image fusion using swarm and physics-based optimization algorithms

In this paper, we propose a comprehensive approach for multi-focus image fusion by leveraging the power of swarm and physics-based optimization algorithms. Our devised fusion scheme, outlined in Fig. 1, focuses on rectifying out-of-focus images through the utilization of advanced optimization techniques. To initiate the process, the input images are

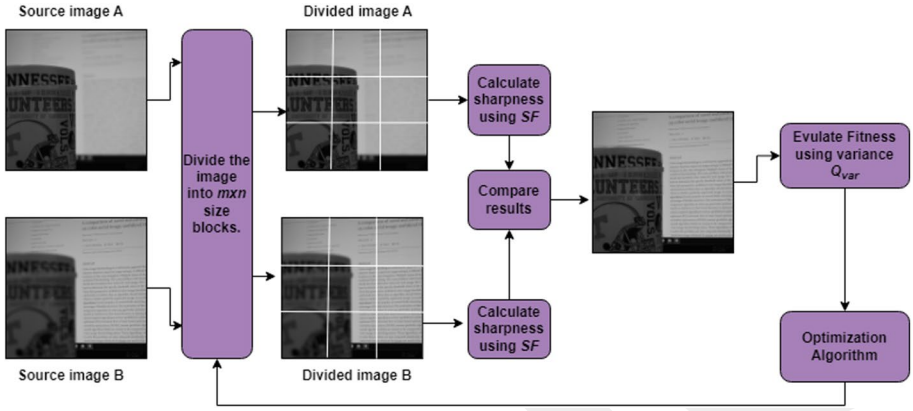

Fig. 1 Multi-focus image fusion schematic diagram by optimization

systematically partitioned into blocks of dimensions $m \times n$, facilitating localized analysis. In this framework, we utilize a carefully developed sharpness metric, which precisely calculates the clarity score for each related block pair.

Our strategy's key component is the thoughtful choice of optimal block pairs for fusion. Leveraging the collective intelligence inherent in swarm optimization algorithms, we navigate through the vast solution space to identify the most suitable block pairs with heightened clarity values. This adaptive and collaborative exploration allows us to seamlessly transcend the limitations of individual block assessments.

Subsequently, our framework seamlessly integrates physics-based optimization algorithms instead of swarm-based algorithms. Blocks with higher sharpness values are seamlessly merged into the fused image produced by this intelligent fusion technique, maintaining the most important visual details from each input. Our approach not only rectifies the initial blurriness stemming from out-of-focus conditions but also enhances the overall image quality by capitalizing on the combined strengths of swarm and physics-based optimization. As demonstrated in Fig. 1, the culmination of these endeavors yields a fused image that transcends the limitations of its constituent parts, embodying a harmonious amalgamation of visual clarity and informational integrity.

In this study, a completely sharp fused image of a scene has been obtained by images taken with different focuses by using a block-based image fusion technique powered by metaheuristic optimizers. For obtaining the everywhere-in-focus result image, the optimization algorithms AOA, AOS, EO, ABC, PSO and JSA have been used. The width and height of the block have been optimized by using these algorithms.

The steps of the proposed method for the multi-focus image fusion are given below:

1. **Parameter Configuration and Convergence Criteria Determination:**

Careful control parameter selection and tuning, as well as the formulation of convergence criteria, are performed prior to algorithm running. These important choices guarantee a balanced exploration-exploitation trade-off by directly affecting the algorithm's convergence rate and overall performance.

2. **Initialization of Population:**

The method starts by producing a population of candidate solutions. Within the search space, this collection of probable solutions covers various block size combinations ($m \times n$). These early candidates establish the groundwork for further investigation.

3. **Block Segmentation without Overlap:**

The input image undergoes systematic division into non-overlapping blocks, each with dimensions $m \times n$. The absence of overlap or spacing between these blocks ensures a comprehensive yet non-redundant coverage of the image's spatial information.

4. **Sharpness Assessment via Spatial Frequency (SF):**

For each individual block, the sharpness value is quantified using a spatial frequency metric. This assessment accurately captures the high-frequency content within the block, thus serving as a reliable indicator of the block's visual clarity.

5. **Selective Block Transfer to Fused Image:**

The block with the highest computed sharpness value is designated for inclusion in the fused image. This selective transfer process effectively cherry-picks the most visually distinct and crisp information from the input images, thereby enhancing the overall clarity and detail of the fused image. The fusion process adheres to the following formula for each corresponding block pair in input images A and B:

$$F_i = \begin{cases} A_k & SF_i^A > SF_i^B \\ B_k & SF_i^A < SF_i^B \\ \frac{A_i + B_i}{2} & other \end{cases} \tag{1}$$

where i is the block index.

6. **Fused Image Fitness Calculation using Variance:**

The fitness value of the fused image is determined by evaluating the variance of pixel intensities within the fused image. This comprehensive assessment gauges the diversity and distribution of pixel values, thereby providing an objective measure of image quality:

$$Q_{var}(F) = \frac{1}{M \times N} \sum_{(i,j)} (F(i,j) - \mu)^2 \tag{2}$$

where μ is the average of F, M and N is the size of the F.

7. **Optimization for Maximizing Fitness:**

Leveraging optimization algorithms, the focus shifts towards the maximization of the fitness function $Q_{var}(F)$, which embodies the image quality metric. Swarm and physics-based optimization techniques collaboratively navigate the solution space, striving to identify the optimal combination of block sizes ($m \times n$) that consistently yield the highest variance value, thus attaining the most visually informative and sharp fused image:

The proposed method offers a reliable and cutting-edge solution for multi-focus image fusion through the diligent application of these phases. This strategy successfully overcomes the drawbacks of conventional techniques by mixing swarm and physics-based optimization, producing fused images with improved sharpness, visual clarity, and content that is information-rich.

3 Physics-based optimization algorithms

Physics-based algorithms have been developed by inspiration of the physical phenomenon seen in nature and physical laws. In this study, three different physics-based algorithms are used, namely, AOA, AOS, and EO.

3.1 Archimedes optimization algorithm (AOA)

The AOA is a method that has been proposed referring to the law of Archimedes and presented by Hashim et al. in the literature [42]. The law of Archimedes explains buoyancy, the force that is exerted on an object when that object is immersed in the liquid. The buoyant force is equal to the weight of the liquid that flows out of a container when an object is immersed in a container full of liquid. If the weight of the liquid that flows out of the container is less than the weight of the immersed object, the object sinks. Otherwise, the object floats. In Archimedes' algorithm, the individuals in a population are objects that are immersed in a liquid. These objects have density, mass, and volume [42]. In Fig. 2, Archimedes' optimization algorithm flowchart is shown.

3.2 Atomic orbital search (AOS)

The AOS algorithm has been inspired by the basic principles of quantum mechanics and the orbital model of an atom and has been proposed by Azizi [43]. The electrons are taken not as particles but as waves whose position is indeterminable. The electron can emit energy, this energy can be drawn by the orbit, or the electron can receive energy. There is no specific place in an atom's orbit. The orbits are calculated by a mathematical function that determines the electron's possible location. The electrons here act as if an ever-moving charge cloud. The electrons can be excited by photons, and this leads to an increase in the energy of the electron. In AOS, bonding energy, a specific energy level that is required to take an electron out of the orbit, is determined. Since it is possible in the quantum ladder concept that electrons can move in different energy levels, the energy of an electron may vary. If the energy of an electron is more than the bounding energy, the electron will go to a higher energy level and if not, the electron will stay in the same energy level or fall to a lower energy level [43]. In Fig. 3, the AOS algorithm flowchart is shown.

3.3 Equilibrium optimizer (EO)

The inspiration of the EO algorithm is the comparison of the balance of the dynamic mass on a control volume [44]. The mass equilibrium equation is used as a function of various sources and leakage mechanisms to define a nonreactive concentration of a component.

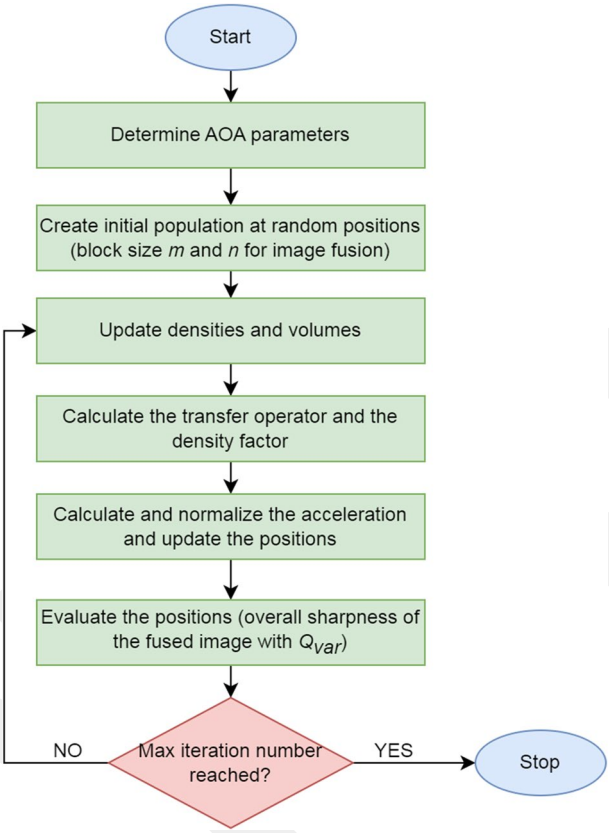

Fig. 2 Implementation flowchart of AOA to multi-focus image fusion

The mass equilibrium equation ensures the law of conservation of mass in a control volume [44]. Figure 4 shows the EO optimization algorithm flowchart.

4 Swarm-based optimization algorithms

A swarm is defined as a set of individuals which are in interact with one another. In a swarm, N representatives work together to achieve a common goal. The swarm-based algorithms that are used in this study are, namely, PSO, ABC, and JSA.

4.1 Particle swarm optimization (PSO)

This optimization algorithm that is developed by Kennedy and Eberhart in 1995 and was influenced by the fact that the animals which live in a swarm act together to satisfy their basic needs such as finding food [45] and is named PSO. The animals that live in a swarm show a set of behaviors for deeds such as finding food and establishing a security perimeter. Such behaviors are realized to be random. By such random behaviors, the animals that belong to a swarm reach their desired goals more efficiently and conveniently. Social information is shared among the members of a swarm, and this is the key principle that

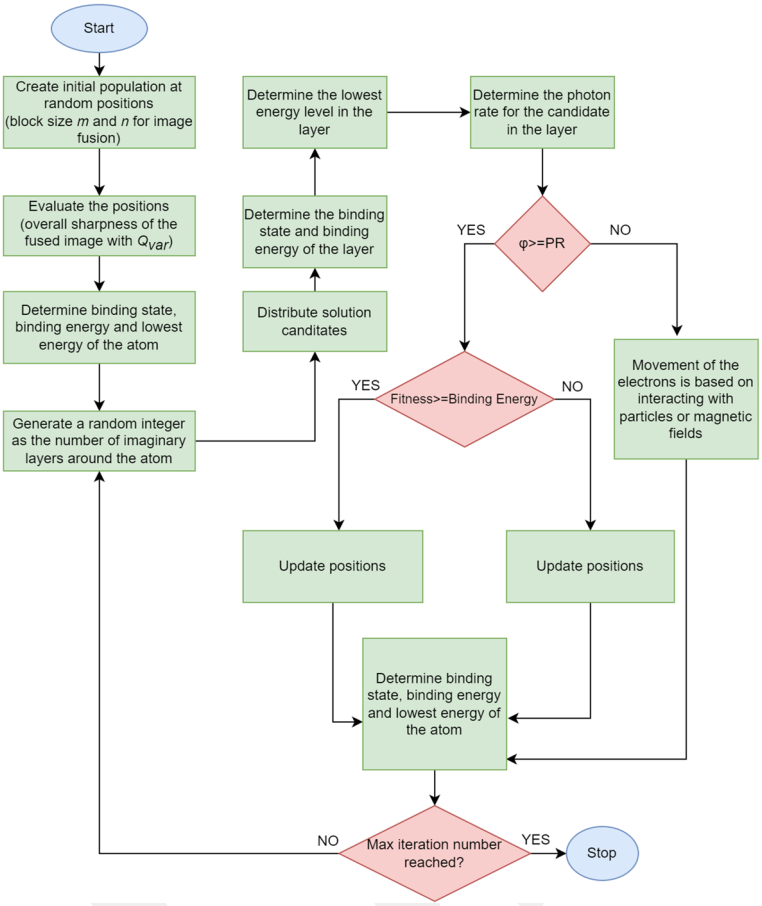

Fig. 3 Implementation flowchart of AOS to multi-focus image fusion

the PSO is based on. The searching procedure is achieved according to the number of generations as it is in genetic algorithms. Each member is named a particle and the flock that consists of these particles is named a swarm. Each particle alters its own location based on its previous experiences toward the best possible position for that particle. The individuals of a swarm change their location according to the best possible position in a swarm. This tendency to move toward the best position is the principle that PSO is based upon. The speed of approach is determined randomly and most of the time the members of a swarm end up in a better position when compared to their previous position. This goes on until the member reaches their goal [45]. In Fig. 5, PSO algorithm flowchart is illustrated.

4.2 Artificial bee Colony (ABC)

In the algorithm, some basic principles that explain the number of the bees that have different tasks in a colony such as the number of food sources indicating the number of employed bees and the number of employed bees is equal to the number of onlookers. As the food in a particular source starts to get depleted the employed bees become

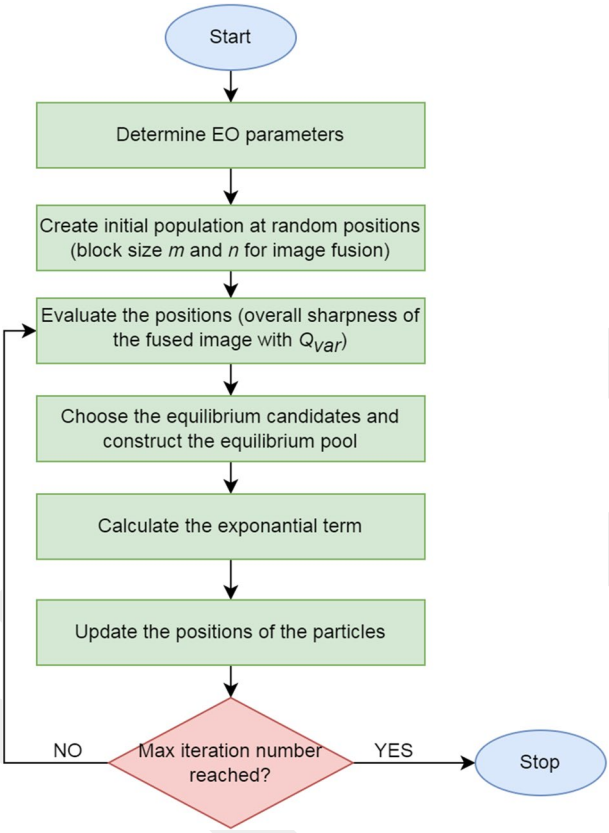

Fig. 4 Implementation flowchart of EO to multi-focus image fusion

scouts. The position of the food source in the colony indicates the possible ways to solve a problem and the amount of nectar indicates the effectiveness of the solution. The desired conclusion is to find the best solution to a problem, which the ABC algorithm tries to find by finding a source that has the most nectar. It also tries to find the minimum and the maximum points of the solution to the problem [46]. In Fig. 6, ABC optimization algorithm flowchart is given.

4.3 Jellyfish search algorithm (JSA)

The JSA is a metaheuristic algorithm that is inspired by a set of behavior that the Jellyfish performs in the ocean [47]. The searching behavior of a Jellyfish mainly consists of behaviors given as: following the currents of the ocean, performing the active and the passive movements in a swarm, approximating the position relative to the Jellyfish flowers, and the control mechanism that allows a Jellyfish to switch back and forth among these movements. Inspired by this set of movements performed by a Jellyfish while searching in the ocean, the JSA has been developed. JSA is based on three rules [47]. Figure 7 shows the JSA flowchart.

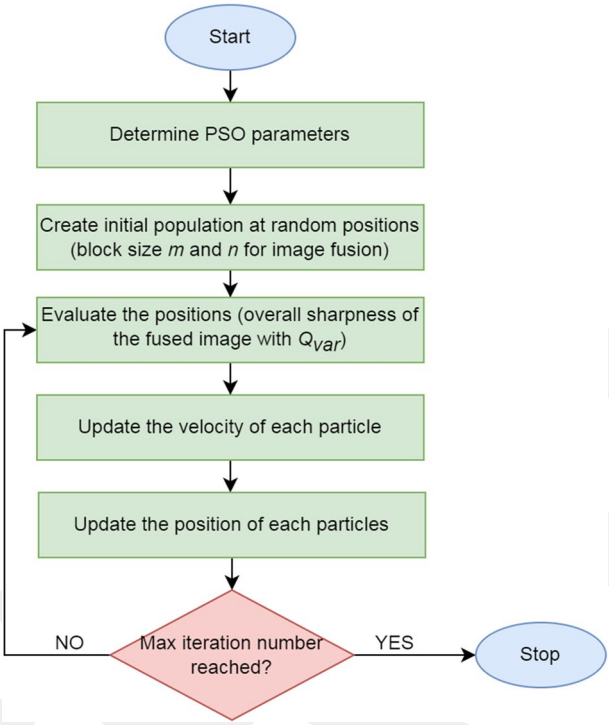

Fig. 5 Implementation flowchart of PSO to multi-focus image fusion

1. Time Control Mechanism: The Jellyfish either follows the current of the ocean or moves in the swarm. The switch that is responsible for switching between this behavior is controlled by a mechanism that is called a Time Control Mechanism.
2. The current of Ocean: The Jellyfish, to seek out food, moves around in the ocean. The greater the amount of food, the greater the power of attraction for the Jellyfish.
3. The amount of food is determined by the function of the location and the objective.

5 Objective evaluation metrics

In this section, objective metrics which are used to evaluate the quality of the result images of the methods quantitatively are given.

5.1 Normalized mutual information (Q_{NMI})

The instabilities in a fused image can be overcome by different methods. One of those methods, which was introduced by Hossny et al. [48] is based on information theory. This metric, which is more redundant to overcome the problems than the conventional metrics based on traditional mutual information, proposes a solution to the problem of instability by using a metric based on normalization [49]. The metric Q_{NMI} is defined as:

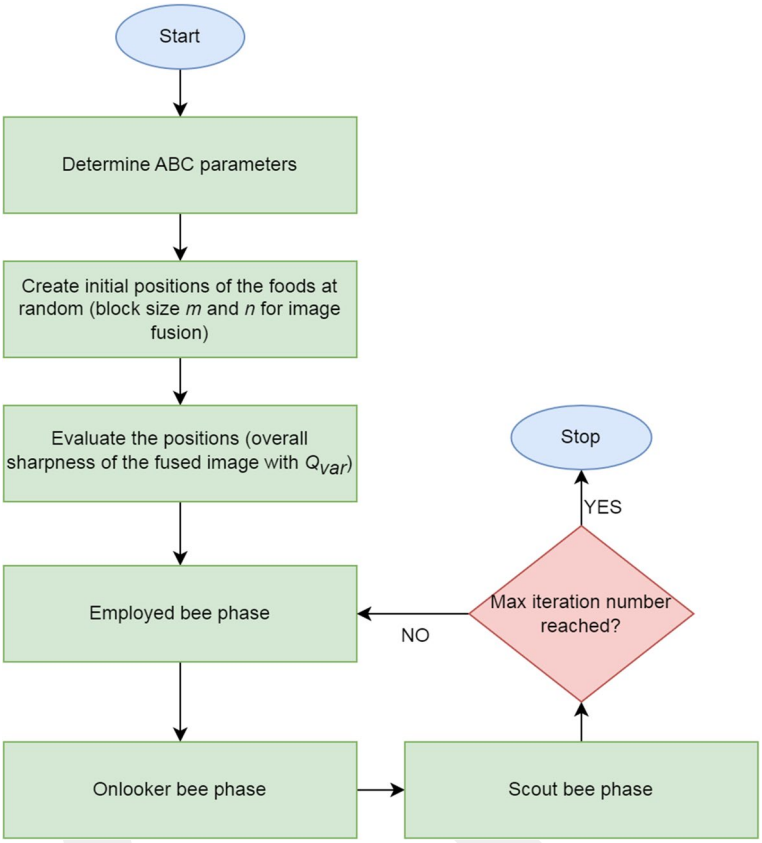

Fig. 6 Implementation flowchart of ABC to multi-focus image fusion

$$Q_{NMI} = 2\left[\frac{MI(A,F)}{H(A)+H(F)} + \frac{MI(B,F)}{H(B)+H(F)}\right] \tag{3}$$

where $H(X)$ denotes the entropy of image X and $MI(A, B)$ is the mutual information between two images A and B [48].

5.2 Edge based quality metric ($Q_P^{AB/F}$)

For images that have the size of $N \times M$, the output image F which is obtained by operating the fusion process (denoted as P) on the input images A and B is obtained as given below:

$$Q_P^{AB/F} = \frac{\sum_{n=1}^{N}\sum_{m=1}^{M} Q^{AF}(n,m)w^A(n,m) + Q^{BF}(n,m)w^B(n,m)}{\sum_{i=1}^{N}\sum_{j=1}^{M}\left(w^A(i,j) + w^B(i,j)\right)} \tag{4}$$

It should be noted that the edge preservation values, $Q^{AF}(n,m)$ and $Q^{BF}(n,m)$, are weighted by $w^A(n,m)$ and $w^B(n,m)$,respectively [50].

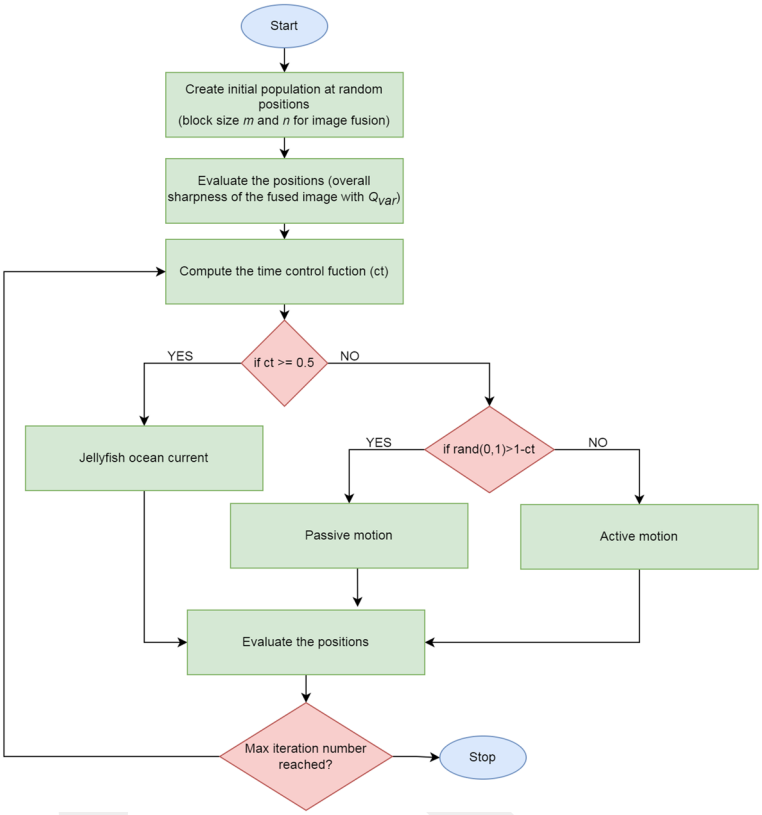

Fig. 7 Implementation flowchart of JSA to multi-focus image fusion

5.3 Sum of the correlations of differences (Q_{SCD})

Among the quality metrics that are used in image fusion, *SCD* is an important metric. By obtaining the difference image, which is defined as computing the similarity between the input and the fused images. This metric does not calculate the quality of the fused image. Instead, it evaluates the quality of the fused image based on the impact of the input image on the fused image [51].

S_1 and S_2 source image, F fusion image, D_1 ve D_2 difference image:

$$QSCD = \mathrm{r}\left(D_1, S_1\right) + \mathrm{r}\left(D_2, S_2\right) \tag{5}$$

where r(.) function calculates correlation between

$$\mathrm{r}\left(D_\mathrm{k}, S_\mathrm{k}\right) = \frac{\sum_i \sum_j \left(\mathrm{D_k}(i,j) - \overline{D}_\mathrm{k}\right)\left(\mathrm{S_k}(i,j) - \overline{S}_\mathrm{k}\right)}{\sqrt{\sum_i \sum_j \left(\mathrm{D_k}(i,j) - \overline{D}_\mathrm{k}\right)^2 \sum_i \sum_j \left(\mathrm{S_k}(i,j) - \overline{S}_\mathrm{k}\right)^2}} \tag{6}$$

5.4 Structural similarity-based metric (Q_y)

Q_y metric has been proposed by Yang et al. for the purpose of measuring the amount of preservation of the structural similarities of the input image in the fused image [52]:

$$Qy(x,y,f|w) = \begin{cases} \{\lambda(w)SSIM(x,,f|w) + \Big(1-\lambda(w)SSIM(y,f|w), \\ \quad if\ SSIM(x,y|w) \geq 0,75, \\ \max\{SSIM(x,f|\ w), SSIM(y,f|\ w)\}, \\ \quad if\ SSIM(x,y|w) < 0,75. \end{cases} \tag{7}$$

5.5 Human perception inspired metric (Q_{CB})

Chen-Blum metric which is inspired by the five senses of a human being consists of five basic steps, namely, filtering the contrast sensitivity, calculating the local contrast, calculating the location of the contrast, creating the map of emphasis and global quality map [53]. The value of the metric is calculated by the mean value of the quality map:

$$QCB(x,y) = \lambda_A(x,y)\ Q_{AF}(x,y) + \lambda_B(x,y)Q_{BF}(x,y) \tag{8}$$

5.6 Spatial frequency (Q_{SF})

The spatial frequency metric is expressed by the calculation of the first-order derivative-based row and column edges of the fused image [54, 55]:

$$Q_{SF} = \sqrt{RF^2 + CF^2} \tag{9}$$

$$RF = \left[\frac{1}{MxN}\sum_{i=1}^{M}\sum_{j=1}^{N}(F(i,j) - F(i,j-1))^2\right]^{1/2} \tag{10}$$

$$CF = \left[\frac{1}{MxN}\sum_{i=1}^{M}\sum_{j=1}^{N}(F(i,j) - F(i-1,j))^2\right]^{1/2} \tag{11}$$

where RF and CF are the row and column frequencies of the F, calculated by the first order derivatives of the adjacent pixels.

5.7 Standard deviation (Q_{STD})

Size of the fused image M and N, where $\overline{F}$ is the mean of the fused image and F is the fused image [56]:

$$QSTD = \left[\frac{1}{MxN}\sum_{i=1}^{M}\sum_{j=1}^{N}\left(F(i,j) - \overline{F}\right)^2\right]^{1/2} \tag{12}$$

5.8 Blind/reference-less image spatial quality evaluator (BRISQUE) (Q_{BRQ})

It is a reference-less image quality metric used to evaluate image quality in the spatial domain. This metric works in three phases. First, the natural scene statistics of the digital image are extracted, then the feature vectors are calculated and finally, the quality value of the image is calculated. For the BRISQUE quality metric, the numeric value is requested to be small. It is a reference-less image quality metric used to evaluate image quality in the spatial domain [57, 58].

6 Experiments

The performance comparison of the physics-based and swarm-based optimization algorithms in multi-focus image fusion has been made in this section. The performances of AOA, AOS, EO, PSO, ABC, and JSA have been compared by using 8 different objective quality metrics such as Q_{NMI} [59], $Q_P^{AB/F}$ [50], Q_{SCD} [51], Q_y [52], Q_{CB} [53], Q_{SF} [54, 55], Q_{STD} [56], Q_{BRQ} [57, 60] on two multi-focus image pairs (520×520 in resolution) taken from Lytro dataset [15] and two multi-focus image pairs (512×512 in resolution) taken in a laboratory environment by our team. Each algorithm has been run 30 times and the average values have been taken. The standard deviation for running the algorithms 30 times has also been calculated. Moreover, the CPU time consumptions of the algorithms are also compared. The lesser the Q_{BRQ} quality metric value means the higher the quality. For other metrics, as the value gets higher so does the quality. In addition, in this study, in order to better see the fusion performance of the algorithms, the numerical and visual results of the methods are also evaluated with the well-known traditional methods in the literature: DWT [25], DCT [29], SWT [4, 27, 28], PCA [35, 61], DWTPCA [62], SWTDCT [63], DCHWT [30], APCA [64, 65]. The experiments have been run on a laptop that has 16 GB of memory, a 2.27 GHz Intel Core i5 processor with MATLAB software. Pre-processing tasks while preparing an image dataset is very important in image processing applications [66, 67].

6.1 Numerical results

In Figs. 8, 4 different input image sets are given. The input image pairs (a) and (b), and (c) and (d) are images that belong to Lytro data set [15] and the pairs (e) and (f), and (g) and (h) are taken using Nikon D3500.

In Table 1, the parameters that belong to the algorithms used in this study are given. The default parameters offered by the original creators of the algorithms are used in the experiments.

In Table 2, the numerical fusion results of the experiment for images (a) and (b) shown in Fig. 8 are given. In the following tables, the methods that achieve the best results for each metric are highlighted in bold. When the physics-based algorithms AOA, AOS, EO and the swarm-based algorithms, PSO, JSA and ABC are compared, it has been realized that the swarm-based algorithms show better performance when compared to physics-based algorithms. Among the swarm-based algorithms, JSA algorithm has the best performance when the Q_{NMI}, $Q_P^{AB/F}$, Q_y, Q_{CB} and Q_{BRQ} quality metrics are concerned. AOS has the best performance when the CPU time consumption is concerned.

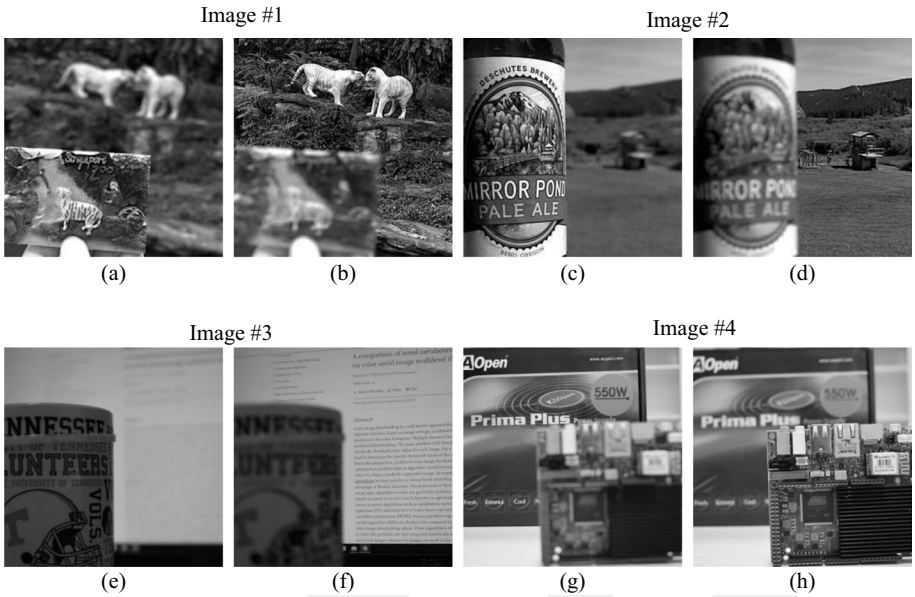

Fig. 8 Test images used in the experiments: Image #1 (**a** and **b**), Image #2 (**c** and **d**), Image #3 (**e** and **f**) and Image #4 (**g** and **h**)

In Table 3, the numerical fusion results of the experiment for images (c) and (d) shown in Fig. 8 are given. It has been realized that the swarm-based algorithms show better fusion performances. ABC and JSA has the best results for all quality metrics. The fastest algorithm is AOS and the slowest algorithm is EO when the CPU time consumption is concerned.

In Table 4, the numerical fusion results of the experiment for images (e) and (f) shown in Fig. 8 are given. When the fusion performances of the algorithms are concerned, AOS algorithm has the best performance for Q_{SF} and Q_{BRQ} metrics, PSO algorithm has the best performance for Q_{NMI} and $Q_P^{AB/F}$ metrics and the ABC algorithm has the best performance for Q_y and Q_{CB} metrics. The fastest algorithm is, again, AOS.

In Table 5, the numerical fusion results of the experiment for images (g) and (h) shown in Fig. 8 are given. It has been realized that the physics-based EO algorithm has the best fusion performance for Q_{SCD}, Q_{CB}, Q_{STD} and Q_{BRQ} quality metrics. For Q_{NMI} and Q_y metrics, ABC has the best fusion performance and for $Q_P^{AB/F}$ and Q_{SF} metrics,

Table 1 Parameters that belong to the algorithms used in the experiments

Algorithm	Parameters
AOA	C3 = 1; C4 = 2;
AOS	LayerNumber = 5; FotonRate = 0.1;
EO	–
PSO	c1 = 1; c2 = 2; wdamp = 1;
ABC	onlooker_count = 4; max_acceleration = 0.5;
JSA	–

Table 2 The numerical fusion results of images (a) and (b) given in Fig. 8 using meta-heuristic optimization methods

Image #1	Q_{NMI}	$Q_P^{AB/F}$	Q_{SCD}	Q_y	Q_{CB}	Q_{SF}	Q_{STD}	Q_{BRQ}	CPU time (sec)
AOA mean	10,437	0,7437	**0,7160**	0,9906	0,8451	37,5449	57,4555	95,463	26,0483
AOA std	0,0000	0,0000	0,0004	0,0001	0,0007	0,0042	0,0045	0,1799	41,109
AOS mean	10,437	0,7436	0,7154	0,9903	0,8441	37,5513	57,4486	98,212	**14,508**
AOS std	0,0000	0,0000	0,0000	0,0000	0,0000	0,0000	0,0000	0,0000	0,8452
EO mean	**10,440**	0,7436	**0,7160**	0,9906	0,8452	37,5373	**57,4560**	90,376	43,8775
EO std	0,0008	0,0004	0,0008	0,0003	0,0011	0,0108	0,0069	10,668	11,5783
PSO mean	10,437	0,7437	0,7152	0,9907	**0,8456**	37,5189	57,4493	89,449	17,3448
PSO std	0,0004	0,0002	0,0015	0,0001	0,0001	0,0357	0,0128	0,6846	89,142
JSA mean	**10,440**	**0,7438**	0,7149	**0,9908**	**0,8456**	37,5017	57,4473	**88,500**	88,270
JSA std	0,0004	0,0001	0,0010	0,0001	0,0002	0,0381	0,0074	0,6537	32,690
ABC mean	10,438	0,7437	**0,7160**	0,9907	0,8454	37,5403	57,4553	94,411	10,3776
ABC std	0,0000	0,0001	0,0004	0,0001	0,0004	0,0058	0,0042	0,2476	0,5621

AOS has the best performance. As far as the CPU time consumption is concerned, AOS is the fastest and EO is the slowest algorithm.

In Table 6, the numerical results of the traditional methods for Image #1 are given. DCT method has the best results according to Q_{nmi}, $Q_p^{AB\_F}$, Q_y, Q_{cb}, Q_{sf}, DWT method has the best results according to Q_{scd}, Q_{std} quality metrics. Moreover, in terms of CPU time consumption PCA is the fastest with 0.0058 seconds.

The numerical results of the traditional methods are given in Table 7 for Image #2. DCT method has the best results according to Q_{nmi}, $Q_p^{AB\_F}$, Q_y, Q_{cb}, Q_{sf}, DWT method has the best results according to Q_{scd}, Q_{std} quality metrics. Furthermore, in terms of CPU time consumption PCA is the fastest with 0.0052 seconds.

Table 3 The numerical fusion results of images (c) and (d) given in Fig. 8 using meta-heuristic optimization methods

Image #2	Q_{NMI}	$Q_P^{AB/F}$	Q_{SCD}	Q_y	Q_{CB}	Q_{SF}	Q_{STD}	Q_{BRQ}	CPU time (sec)
AOA mean	**11,622**	0,7513	0,6263	**0,9885**	**0,8440**	36,3776	60,2618	72,862	67,601
AOA std	0,0005	0,0003	0,0003	0,0001	0,0002	0,0142	0,0017	0,5696	25,069
AOS mean	11,573	0,7474	0,6152	0,9871	0,8393	36,2702	60,1987	12,5087	**12,260**
AOS std	0,0000	0,0000	0,0000	0,0000	0,0000	0,0000	0,0000	0,0000	0,0384
EO mean	11,610	0,7509	0,6252	**0,9885**	0,8429	36,3408	60,2593	92,160	21,7115
EO std	0,0016	0,0008	0,0011	0,0002	0,0014	0,0361	0,0027	21,633	12,9966
PSO mean	11,612	0,7507	0,6255	0,9884	0,8436	36,3510	60,2571	83,566	79,246
PSO std	0,0012	0,0009	0,0010	0,0002	0,0005	0,0404	0,0045	15,689	26,187
JSA mean	**11,622**	**0,7514**	**0,6264**	**0,9885**	**0,8440**	**36,3803**	**60,2621**	**71,804**	47,555
JSA std	0,0000	0,0000	0,0000	0,0000	0,0000	0,0000	0,0000	0,0000	0,2377
ABC mean	**11,622**	**0,7514**	**0,6264**	**0,9885**	**0,8440**	**36,3803**	**60,2621**	**71,804**	90,059
ABC std	0,0000	0,0000	0,0000	0,0000	0,0000	0,0000	0,0000	0,0000	0,3023

Table 4 The numerical fusion results of images (e) and (f) given in Fig. 8 using meta-heuristic optimization methods

Image #3	Q_{NMI}	$Q_P^{AB/F}$	Q_{SCD}	Q_y	Q_{CB}	Q_{SF}	Q_{STD}	Q_{BRQ}	CPU time (sec)
AOA mean	12,950	0,7524	0,2637	0,9877	0,8059	14,9455	60,8416	36,6519	89,139
AOA std	0,0034	0,0033	0,0015	0,0004	0,0032	0,0315	0,0057	0,6368	40,951
AOS mean	12,918	0,7707	0,2480	0,9860	0,7891	**15,0348**	60,7602	**34,1252**	**15,080**
AOS std	0,0000	0,0000	0,0000	0,0000	0,0000	0,0000	0,0000	0,0000	0,1217
EO mean	12,741	0,7132	0,2641	0,9845	0,7629	14,4835	60,8587	34,6208	17,5701
EO std	0,0154	0,0578	0,0053	0,0038	0,0427	0,6378	0,0144	33,129	15,4957
PSO mean	**12,973**	**0,7563**	0,2637	0,9874	0,8046	14,9774	60,8392	36,1082	92,728
PSO std	0,0065	0,0085	0,0031	0,0007	0,0043	0,0735	0,0123	13,561	70,532
JSA mean	12,918	0,7512	**0,2654**	0,9877	0,8061	14,9393	**60,8485**	37,0975	53,597
JSA std	0,0012	0,0004	0,0006	0,0001	0,0009	0,0074	0,0015	0,1264	0,6280
ABC mean	12,936	0,7516	0,2645	**0,9878**	**0,8063**	14,9413	60,8446	36,9290	92,762
ABC std	0,0022	0,0006	0,0005	0,0001	0,0009	0,0098	0,0016	0,2405	0,4079

Table 5 The numerical fusion results of images (g) and (h) given in Fig. 8 using meta-heuristic optimization methods

Image #4	Q_{NMI}	$Q_P^{AB/F}$	Q_{SCD}	Q_y	Q_{CB}	Q_{SF}	Q_{STD}	Q_{BRQ}	CPU time (sec)
AOA mean	11,687	0,7184	0,4801	0,9839	0,7710	30,7069	63,5638	19,4724	68,104
AOA std	0,0023	0,0014	0,0022	0,0004	0,0029	0,0794	0,0119	0,5247	17,701
AOS mean	11,621	**0,7193**	0,4424	0,9759	0,7544	**31,1820**	63,3152	22,9311	13,190
AOS std	0,0000	0,0000	0,0000	0,0000	0,0000	0,0000	0,0000	0,0000	0,1596
EO mean	11,685	0,7171	**0,4828**	0,9824	**0,7740**	30,7128	**63,6270**	**18,7635**	11,1951
EO std	0,0023	0,0043	0,0060	0,0019	0,0053	0,1917	0,0420	11,682	48,285
PSO mean	11,708	0,7186	0,4803	0,9837	0,7713	30,7186	63,5642	19,3265	51,273
PSO std	0,0019	0,0017	0,0021	0,0005	0,0033	0,1069	0,0126	0,5367	0,6333
JSA mean	11,708	0,7171	0,4817	**0,9840**	0,7705	30,6254	63,5705	19,6493	52,677
JSA std	0,0022	0,0012	0,0009	0,0002	0,0010	0,0723	0,0049	0,2633	0,7325
ABC mean	**11,715**	0,7166	0,4820	**0,9840**	0,7703	30,5971	63,5715	19,6492	88,429
ABC std	0,0024	0,0010	0,0008	0,0001	0,0004	0,0592	0,0043	0,1410	0,2964

Table 6 The numerical fusion results of images (a) and (b) given in Fig. 8 using traditional fusion methods

Image #1	Q_{NMI}	$Q_P^{AB/F}$	Q_{SCD}	Q_y	Q_{CB}	Q_{SF}	Q_{STD}	Q_{BRQ}	CPU time (sec)
DWT_PCA	0,7896	0,6368	0,4727	0,9830	0,7664	29,8626	54,7031	31,0853	0,0843
DCHWT	0,6855	0,7119	0,6691	0,9825	0,7719	35,8542	56,2683	10,0283	21,546
APCA	0,6281	0,6282	0,4337	0,9404	0,7056	26,4388	53,0714	26,9801	0,3562
DCT	**10,449**	**0,7414**	0,7053	**0,9908**	**0,8451**	**37,4225**	57,3749	70,939	0,2889
PCA	0,6087	0,5505	0,4726	0,8774	0,7077	21,3494	52,4159	10,4694	**0,0058**
DWT	0,6093	0,6936	**0,7808**	0,9720	0,7481	37,1565	**57,8570**	15,7194	0,3127
SWT_DCT	0,6575	0,5366	0,5342	0,9083	0,6613	35,9037	55,8426	18,9314	38,963
SWT	0,6072	0,6714	0,5738	0,9582	0,7063	32,8369	54,4338	**60,706**	0,1146

Table 7 The numerical fusion results of images (c) and (d) given in Fig. 8 using traditional fusion methods

Image #2	Q_{NMI}	$Q_P^{AB/F}$	Q_{SCD}	Q_y	Q_{CB}	Q_{SF}	Q_{STD}	Q_{BRQ}	CPU time (sec)
DWT_PCA	0,9405	0,6179	0,4532	0,9818	0,7406	30,0072	57,9438	31,7882	0,0182
DCHWT	0,8285	0,7014	0,5932	0,9766	0,7495	34,6818	59,2271	14,709	19,197
APCA	0,7869	0,5392	0,4274	0,8990	0,6952	20,5065	55,7949	10,7317	0,3777
DCT	**11,609**	**0,7486**	0,6166	**0,9881**	**0,8422**	**36,1707**	60,2185	12,2396	0,2716
PCA	0,7934	0,5489	0,4528	0,8979	0,7010	20,4687	55,9092	71,182	**0,0052**
DWT	0,7629	0,6901	**0,7692**	0,9642	0,7400	35,6547	**61,1191**	50,174	0,2025
SWT_DCT	0,8060	0,5301	0,5009	0,9190	0,6666	34,0343	59,0298	**0,1499**	39,390
SWT	0,7875	0,6743	0,5470	0,9615	0,7090	31,2676	57,7688	10,7011	0,1108

Table 8 The numerical fusion results of images (e) and (f) given in Fig. 8 using traditional fusion methods

Image #3	Q_{NMI}	$Q_P^{AB/F}$	Q_{SCD}	Q_y	Q_{CB}	Q_{SF}	Q_{STD}	Q_{BRQ}	CPU time (sec)
DWT_PCA	11,444	0,6061	0,2027	0,9824	0,7035	11,2948	60,0060	41,9770	0,0239
DCHWT	10,282	0,7295	0,2482	0,9831	0,7288	14,4050	60,6004	39,8980	19,835
APCA	10,007	0,6097	0,2192	0,9400	0,6296	94,755	60,0964	37,7211	0,3572
DCT	**13,387**	**0,7666**	0,2057	**0,9861**	**0,8011**	14,7898	60,5779	34,6028	0,2787
PCA	0,9956	0,5533	0,1885	0,9134	0,5996	86,488	60,0540	37,8243	**0,0065**
DWT	0,9689	0,7294	**0,3779**	0,9807	0,7460	**15,0751**	**61,2897**	38,1867	0,2352
SWT_DCT	0,9208	0,5139	0,1829	0,9108	0,5644	14,2445	60,4824	**29,6015**	39,994
SWT	0,9337	0,6711	0,2561	0,9593	0,6067	12,7742	60,3687	35,4126	0,0963

Table 9 The numerical fusion results of images (g) and (h) given in Fig. 8 using traditional fusion methods

Image #4	Q_{NMI}	$Q_P^{AB/F}$	Q_{SCD}	Q_y	Q_{CB}	Q_{SF}	Q_{STD}	Q_{BRQ}	CPU time (sec)
DWT_PCA	0,9261	0,6629	0,4115	0,9768	0,7376	22,9352	61,7034	31,2591	0,0163
DCHWT	0,7835	0,6665	0,4952	0,9592	0,6837	28,6596	62,4354	25,3107	20,332
APCA	0,8116	0,6473	0,4028	0,9436	0,7051	21,1880	60,9371	30,7524	0,3630
DCT	**11,705**	**0,7195**	0,4636	**0,9835**	**0,7755**	30,8964	63,4514	18,1928	0,3018
PCA	0,8221	0,5933	0,4143	0,9077	0,7062	19,1147	60,6787	**17,1136**	**0,0039**
DWT	0,7262	0,6493	**0,6904**	0,9427	0,6878	**31,1928**	**65,2548**	23,0095	0,1945
SWT_DCT	0,8643	0,5713	0,4774	0,9166	0,6744	29,4674	63,4496	22,7784	39,136
SWT	0,7996	0,6750	0,5081	0,9560	0,7024	27,1198	61,9997	20,7815	0,0866

In Table 8, the numerical results of the traditional methods for Image #3 are given. DCT method has the best results according to Q_{nmi}, $Q_p^{AB\_F}$, Q_y, Q_{cb}, DWT method has the best results according to Q_{scd}, Q_{sf}, Q_{std} quality metrics. Moreover, in terms of CPU time consumption PCA is the fastest with 0.0065 seconds.

The numerical results of the traditional methods are given in Table 9 for Image #4. DCT method has the best results according to Q_{nmi}, $Q_p^{AB\_F}$, Q_y, Q_{cb}, DWT method has the best results according to Q_{scd}, Q_{sf}, Q_{std} quality metrics. Furthermore, in terms of CPU time consumption PCA is the fastest with 0.0039 seconds.

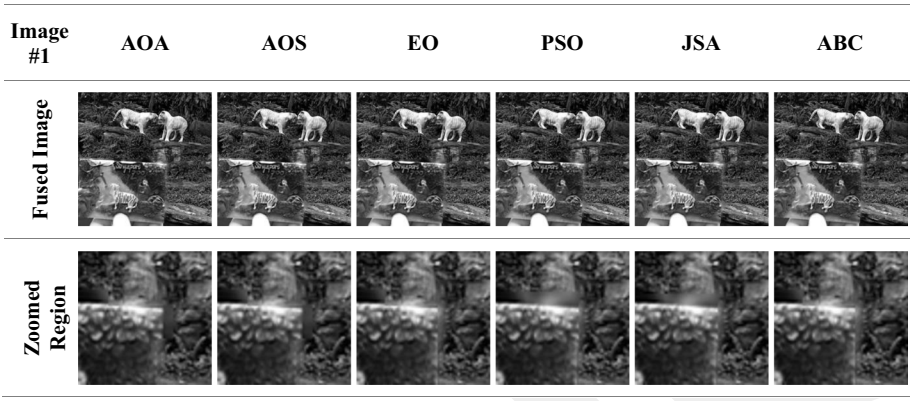

Fig. 9 Fused image and a zoomed region of Image #1 using meta-heuristic optimization methods

6.2 Visual results

In multi-focus image fusion, it is stated that the quantitative analysis itself is not sufficient enough and in addition to the quantitative analysis, a subjective analysis on the visual results is also required. In this section, the visual results obtained from the experiments are given. Figures 9 and 10 consist of the visual results of the image pairs (a) and (b), (c) and (d) that are taken from the Lytro dataset shown in Fig. 8. In addition to these, Figs. 11 and 12 consist of the visual results of the image pairs (e) and (f), (g) and (h) that are captured with Nikon D3500 digital camera, shown in from Fig. 8.

In Fig. 9, the fused images of (a) and (b) from Fig. 8 are given. Also, a zoomed portions of the result image are given for detailed visual analysis. Among the fused images, it is realized that EO and ABC algorithms have shown a near-perfect performance.

In Fig. 10, the fused images of (c) and (d) from Fig. 8 are given. Among the fused images, it is realized that AOA, EO, JSA and ABC algorithms have shown a better performance. It is also realized that the algorithms AOS and PSO have some blurry regions in the fused image.

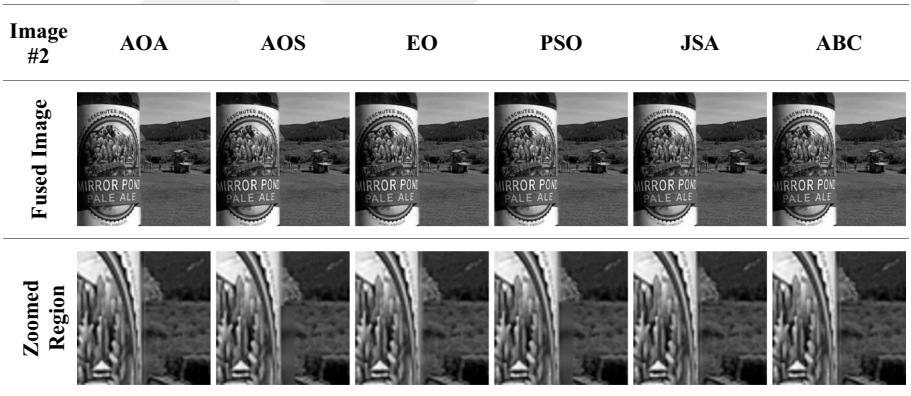

Fig. 10 Fused image and a zoomed region of Image #2 using meta-heuristic optimization methods

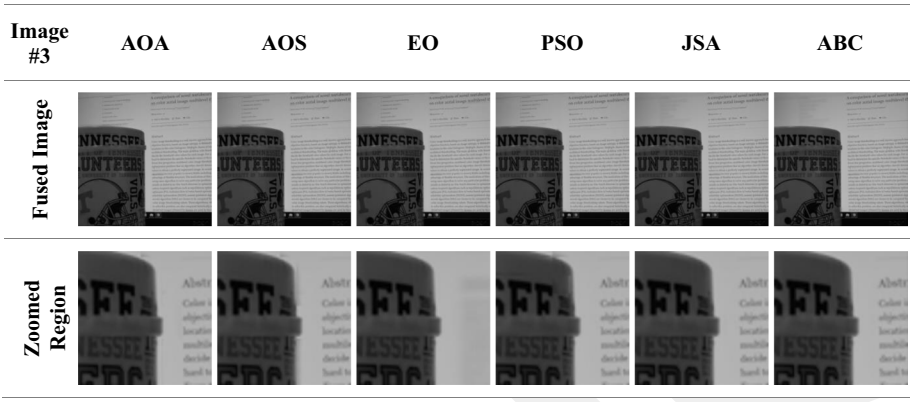

Fig. 11 Fused image and a zoomed region of Image #3 using meta-heuristic optimization methods

In Fig. 11, the fused images of (e) and (f) from Fig. 8 are given. Among the fused images, it is realized that EO has the worst performance. On the other hand, JSA and ABC have better performance than the others.

In Fig. 12, the fused images of (g) and (h) from Fig. 8 are given. Among the fused images, it is realized that the AOA algorithm has worst performance in fusion and the AOS, JSA and ABC algorithm have better performance than others.

The visual outcomes for Images #1, #2, #3, and #4 are effectively showcased in Figs. 13, 14, 15 and 16, presenting the performance of the proposed multi-focus image fusion method. The upper row of each figure aptly displays the resulting fused images, while the lower row provides zoomed-in views, affording a more granular perspective on the finer details. Upon careful observation and consideration of these visual results, a clear trend emerges, highlighting the exceptional efficacy of both the Discrete Cosine Transform (DCT) method and the Discrete Wavelet Transform (DWT) method across all the depicted images.

These two advanced techniques consistently exhibit a good performance in terms of sharpness and clarity when compared to other traditional fusion approaches. The nuances and intricate features of the scenes are more faithfully captured through the

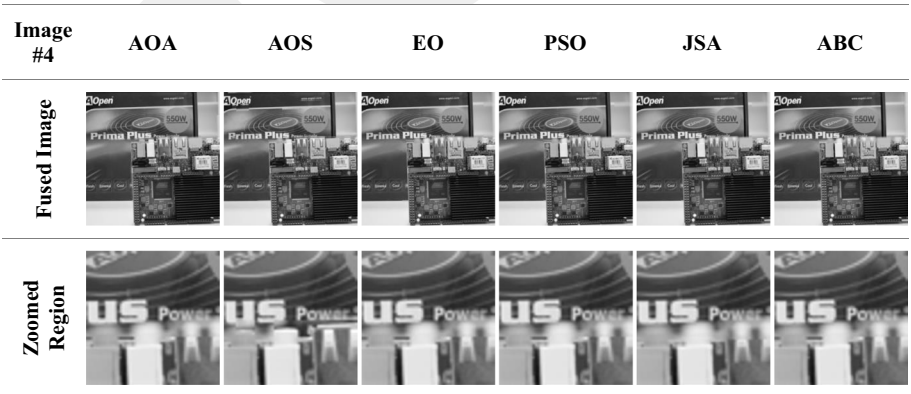

Fig. 12 Fused image and a zoomed region of Image #4 using meta-heuristic optimization methods

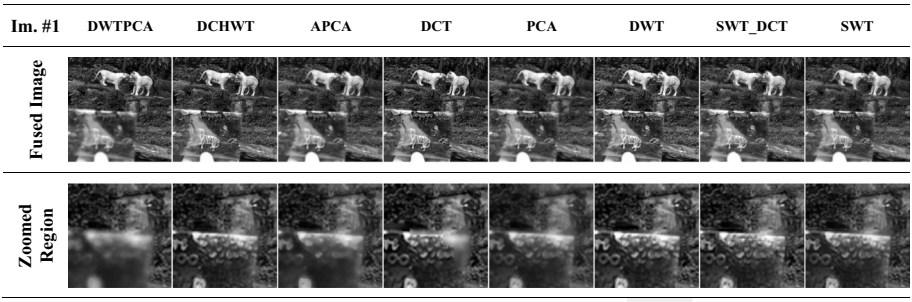

Fig. 13 Fused image and a zoomed region of Image #1 using traditional fusion methods

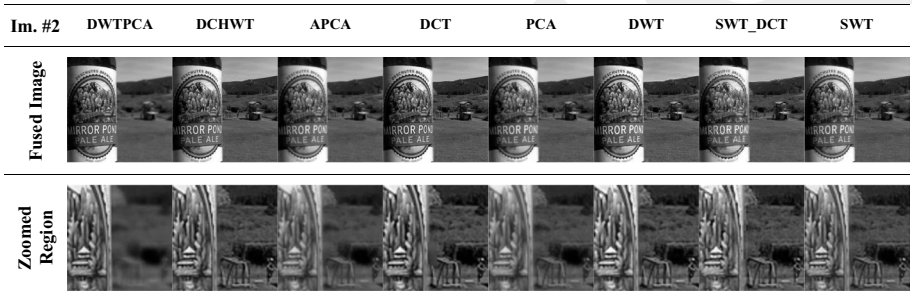

Fig. 14 Fused image and a zoomed region of Image #2 using traditional fusion methods

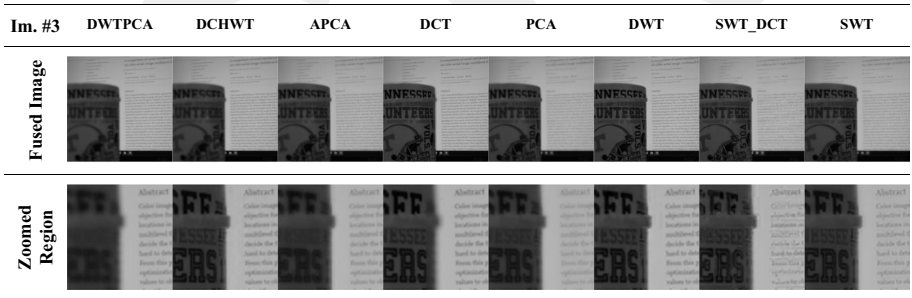

Fig. 15 Fused image and a zoomed region of Image #3 using traditional fusion methods

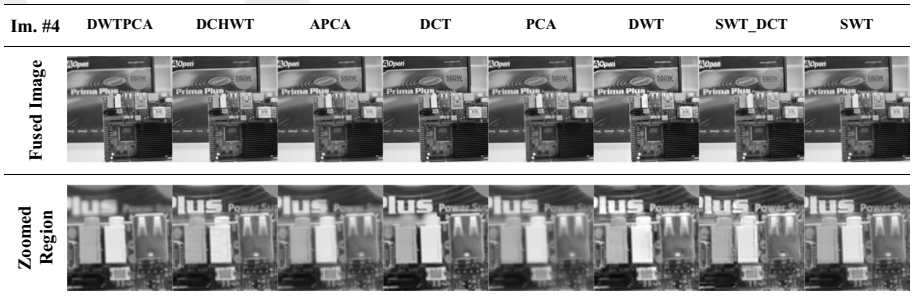

Fig. 16 Fused image and a zoomed region of Image #4 using traditional fusion methods

DCT and DWT methods, yielding fused images that encapsulate a heightened level of visual definition and fidelity. This overarching trend, evident across multiple images, attests to the robustness and superiority of the DCT and DWT methods in preserving the salient details during the fusion process.

7 Conclusion

In this study, multi-focus images are fused by using swarm-based algorithms such as ABC, JSA and PSO and physics-based algorithms such as AOA, AOS and EO. Each algorithm has been run for 30 times and the performance of each algorithm has been tested. The experiments have been conducted upon 4 different image sets, 2 of them are taken from the Lytro dataset and 2 of them are captured by Nikon D3500 digital camera. The results of the experiment have been compared for the qualitative and quantitative performance and as well as the CPU time consumption. The EO algorithm has the best performance for the fusion of the images (a) and (b) given in Fig. 8. The JSA and ABC algorithms has the best performance for the fusion of the images (c) and (d) given in Fig. 8. For the fusion of (e) and (f), JSA and ABC algorithms show the best performances for different quality metrics. The AOS and ABC algorithm have the best performance for the fusion of the images (g) and (h) given in Fig. 8. As a result, the ABC and JSA optimization algorithm has the best fusion performance among the compared optimization algorithms. For all images, DCT and DWT have good performance among the traditional image fusion techniques. When meta-heuristic and traditional methods are compared together, performance of ABC is better than DCT in terms of quality metrics Q_{nmi}, Q_{scd}, Q_y, and Q_{std} in most cases. Visual results of EO and JSA is clearer than DWT for Images #1, #2 and #3. In future studies, multiple quality metrics can be optimized together by using multi-objective mete-heuristic optimization algorithms to improve the overall performance.

Acknowledgements This work is supported by Kayseri University Scientific Research Projects Coordination Unit with the grant number FYL-2021-1051.

Data availability The datasets generated during and/or analyzed during the current study are available from the corresponding author on reasonable request.

Declarations

Competing interests The authors declare that they have no known competing financial interests or personal relationships that could have appeared to influence the work reported in this paper.

References

1. Liu Y, Liu S, Wang Z (2015) Multi-focus image fusion with dense SIFT. Inf Fus 23:139–155
2. Tang H, Xiao B, Li W, Wang G (2018) Pixel convolutional neural network for multi-focus image fusion. Inf Sci 433:125–141
3. Kaur G, Kaur P (2016) "Survey on multifocus image fusion techniques," In 2016 international conference on electrical, electronics, and optimization techniques (ICEEOT), pp. 1420–1424: IEEE. https://ieeexplore.ieee.org/document/7754918

4. Singh S, Patil M (2016) Multifocus image fusion based on spatial frequency and contrast based analysis under stationary wavelet transform domain. Int J Sci Eng Res 7(5):225–230
5. Meher B, Agrawal S, Panda R, Abraham A (2019) A survey on region based image fusion methods. Inf Fus 48:119–132
6. Li Q, Yang X, Wu W, Liu K, Jeon G (2018) Multi-focus image fusion method for vision sensor systems via dictionary learning with guided filter. Sensors 18(7):2143
7. Ghassemian H (2016) A review of remote sensing image fusion methods. Inf Fus 32:75–89
8. Wang Z, Ma Y (2008) Medical image fusion using m-PCNN. Inf Fus 9(2):176–185
9. Song Y, Li M, Li Q, Sun L (2006) A new wavelet based multi-focus image fusion scheme and its application on optical microscopyIn 2006 IEEE International Conference on Robotics and Biomimetics (pp. 401–405). IEEE. https://doi.org/10.1109/ROBIO.2006.340210
10. Wang Z, Ziou D, Armenakis C, Li D, Li Q (2005) A comparative analysis of image fusion methods. IEEE Trans Geosci Remote Sens 43(6):1391–1402
11. Zhi-guo J, Dong-bing H, Jin C, Xiao-kuan Z (2004) A wavelet based algorithm for multi-focus micro-image fusion.In Third International Conference on Image and Graphics (ICIG'04) (pp. 176–179). IEEE. https://doi.org/10.1109/ICIG.2004.29
12. Liu Y, Wang L, Cheng J, Li C, Chen X (2020) Multi-focus image fusion: a survey of the state of the art. Inf Fus 64:71–91
13. Bhat S, Koundal D (2021) Multi-focus image fusion techniques: a survey. Artif Intell Rev 54(8):5735–5787
14. Sahu DK, Parsai M (2012) Different image fusion techniques–a critical review. Int J Mod Eng Res 2(5):4298–4301
15. Nejati M, Samavi S, Shirani S (2015) Multi-focus image fusion using dictionary-based sparse representation. Inf Fus 25:72–84
16. Nejati M et al (2017) Surface area-based focus criterion for multi-focus image fusion. Inf Fus 36:284–295
17. Garg R, Gupta P, Kaur H (2014) Survey on multi-focus image fusion algorithms. In 2014 recent advances in engineering and computational sciences (RAECS) (pp. 1–5). IEEE. https://doi.org/10.1109/RAECS.2014.6799615
18. Li Z, Jing Z, Liu G, Sun S, Leung H (2003) Pixel visibility based multifocus image fusion, in International Conference on Neural Networks and Signal Processing, 2003. Proceedings of the 2003. IEEE 2:1050–1053
19. Chen Y, Guan J, Cham W-K (2017) Robust multi-focus image fusion using edge model and multi-matting. IEEE Trans Image Process 27(3):1526–1541
20. Xia X, Yao Y, Yin L, Wu S, Li H, Yang Z (2018) Multi-focus image fusion based on probability filtering and region correction. Signal Process 153:71–82
21. Aslantas V, Kurban R (2009) A comparison of criterion functions for fusion of multi-focus noisy images. Opt Commun 282(16):3231–3242
22. Huang W, Jing Z (2007) Multi-focus image fusion using pulse coupled neural network. Pattern Recogn Lett 28(9):1123–1132
23. Toprak AN, Aslantaş V (2018) Fusion of multi-focus image by blocks optimal positions. In 2018 3rd International Conference on Computer Science and Engineering (UBMK) (pp. 471–476). IEEE. https://doi.org/10.1109/UBMK.2018.8566416
24. Aslantas V, Toprak AN (2014) Multi focus image fusion by differential evolution algorithm. In 2014 11th international conference on informatics in control, automation and robotics (ICINCO) (vol. 1, pp. 312–317). IEEE. https://doi.org/10.5220/0005061103120317. https://ieeexplore.ieee.org/document/7049787
25. Yang Y (2011) A novel DWT based multi-focus image fusion method. Procedia Eng 24:177–181
26. Patel R, Rajput M, Parekh P (2015) Comparative study on multi-focus image fusion techniques in dynamic scene. Int J Comput Appl 109(6)
27. Kannan K, Perumal SA, Arulmozhi K (2010) Area level fusion of multi-focused images using multi-stationary wavelet packet transform. Int J Comput Appl 2(1):88–95
28. Pradnya PM, Sachin DR (2013) Wavelet based image fusion techniques. In 2013 international conference on intelligent systems and signal processing (ISSP)(pp. 77–81). IEEE. https://doi.org/10.1109/ISSP.2013.6526878
29. Desale RP, Verma SV (2013) Study and analysis of PCA, DCT & DWT based image fusion techniques. In 2013 international conference on signal processing, image processing & pattern recognition (pp. 66–69) IEEE. https://doi.org/10.1109/ICSIPR.2013.6497960
30. Shreyamsha Kumar B (2013) Multifocus and multispectral image fusion based on pixel significance using discrete cosine harmonic wavelet transform. Signal, Image Vid Process 7:1125–1143

31. Vakaimalar E, Mala K (2019) Multifocus image fusion scheme based on discrete cosine transform and spatial frequency. Multimed Tools Appl 78(13):17573–17587
32. Zafar I, Edirisinghe E, Bez H (2006) Multi-exposure & multi-focus image fusion in transform domain. In International Conference on Visual Information Engineering (VIE 2006) (pp. 606-611). IET Conference Proceedings. https://doi.org/10.1049/cp:20060600
33. Haghighat MBA, Aghagolzadeh A, Seyedarabi H (2011) Multi-focus image fusion for visual sensor networks in DCT domain. Comput Electr Eng 37(5):789–797
34. Phamila YAV, Amutha R (2014) Discrete cosine transform based fusion of multi-focus images for visual sensor networks. Signal Process 95:161–170
35. Wan T, Zhu C, Qin Z (2013) Multifocus image fusion based on robust principal component analysis. Pattern Recogn Lett 34(9):1001–1008
36. Bouzos O, Andreadis I, Mitianoudis N (2019) Conditional random field model for robust multi-focus image fusion. IEEE Trans Image Process 28(11):5636–5648
37. Kong J, Zheng K, Zhang J, Feng X (2008) Multi-focus image fusion using spatial frequency and genetic algorithm. Int J Comput Sci Netw Secur 8(2):220–224
38. Aslantas V, Kurban R (2010) Fusion of multi-focus images using differential evolution algorithm. Expert Syst Appl 37(12):8861–8870
39. Banharnsakun A (2019) Multi-focus image fusion using best-so-far abc strategies. Neural Comput & Applic 31(7):2025–2040
40. Çıtıl F, Kurban R, Durmuş A, Karaköse E (2022) Fusion of Multi-Focus Images using Jellyfish Search Optimizer. Eur J Sci Technol (37):147–155. https://doi.org/10.31590/ejosat.1136956
41. Hu Z, Liang W, Ding D, Wei G (2021) An improved multi-focus image fusion algorithm based on multi-scale weighted focus measure. Appl Intell 51(7):4453–4469
42. Hashim FA, Hussain K, Houssein EH, Mabrouk MS, Al-Atabany W (2021) Archimedes optimization algorithm: a new metaheuristic algorithm for solving optimization problems. Appl Intell 51(3):1531–1551
43. Azizi M (2021) Atomic orbital search: a novel metaheuristic algorithm. Appl Math Model 93:657–683
44. Faramarzi A, Heidarinejad M, Stephens B, Mirjalili S (2020) Equilibrium optimizer: a novel optimization algorithm. Knowl-Based Syst 191:105190
45. Eberhart R, Kennedy J (1995) A new optimizer using particle swarm theory. In MHS'95. Proceedings of the sixth international symposium on micro machine and human science (pp. 39–43). IEEE. https://doi.org/10.1109/MHS.1995.494215
46. Karaboga D, Basturk B (2007) A powerful and efficient algorithm for numerical function optimization: artificial bee colony (ABC) algorithm. J Glob Optim 39(3):459–471
47. Chou J-S, Truong D-N (2021) A novel metaheuristic optimizer inspired by behavior of jellyfish in ocean. Appl Math Comput 389:125535
48. Hossny M, Nahavandi S, Creighton D (2008) Comments on'Information measure for performance of image fusion'. Electron Lett 44(18):1066–1067
49. Qu G, Zhang D, Yan P (2002) Information measure for performance of image fusion. Electron Lett 38(7):1
50. Xydeas CS, Petrovic V (2000) Objective image fusion performance measure. Electron Lett 36(4):308–309
51. Aslantas V, Bendes E (2015) A new image quality metric for image fusion: the sum of the correlations of differences. Aeu-Int J Electron Commun 69(12):1890–1896
52. Li S, Hong R, Wu X (2008) A novel similarity based quality metric for image fusion. In 2008 International Conference on Audio, Language and Image Processing (pp. 167–172). IEEE. https://doi.org/10.1109/ICALIP.2008.4589989
53. Chen Y, Blum RS (2009) A new automated quality assessment algorithm for image fusion. Image Vis Comput 27(10):1421–1432
54. Eskicioglu AM, Fisher PS (1995) Image quality measures and their performance. IEEE Trans Commun 43(12):2959–2965
55. Hassen R, Wang Z, Salama MM (2013) Image sharpness assessment based on local phase coherence. IEEE Trans Image Process 22(7):2798–2810
56. Liu Y, Liu S, Wang Z (2015) A general framework for image fusion based on multi-scale transform and sparse representation. Inf Fus 24:147–164
57. Mittal A, Moorthy AK, Bovik AC (2012) No-reference image quality assessment in the spatial domain. IEEE Trans Image Process 21(12):4695–4708
58. Mittal A, Soundararajan R, Bovik AC (2012) Making a "completely blind" image quality analyzer. IEEE Signal Process Lett 20(3):209–212

59. Estévez PA, Tesmer M, Perez CA, Zurada JM (2009) Normalized mutual information feature selection. Trans Neural Netw 20(2):189–201
60. Mittal A, Moorthy AK, Bovik AC (2011) "Blind/referenceless image spatial quality evaluator," In 2011 conference record of the forty fifth asilomar conference on signals, systems and computers (ASILOMAR), pp. 723–727: IEEE
61. Kurita T (2019) "Principal component analysis (PCA)," Comput Vis A Ref Guide pp. 1–4
62. Helonde MRP, Joshi M (2015) Image fusion based on medical images using DWT and PCA methods. J Comput Tech 2(1):76–79. http://www.ijctjournal.org/Vol2IssueNo.1.htm
63. Baraiya S, Gagnani LP (2014) An introduction of image fusion techniques. Int J Innov Res Sci Technol 1(7):86–89
64. Perona P, Malik J (1990) Scale-space and edge detection using anisotropic diffusion. IEEE Trans Pattern Anal Mach Intell 12(7):629–639. https://doi.org/10.1109/34.56205
65. Gerig G, Kubler O, Kikinis R, Jolesz FA (1992) Nonlinear anisotropic filtering of MRI data. IEEE Trans Med Imaging 11(2):221–232
66. Maini S, Aggarwal AK (2018) Camera position estimation using 2D image dataset. Int J Innov Eng Technol (IJIET) 10(2):199–203
67. Aggarwal AK (2015) Autonomous navigation of intelligent Vehiclesusing vision based method. Int J Res Electron Commun Technol 3(5):1–10